Thickness Dependence and Percolation Scaling of Hydrogen Production Rate in MoS_2 Nanosheet and Nanosheet-Carbon Nanotube Composite Catalytic Electrodes

David McAteer,[1] Zahra Gholamvand,[1] Niall McEvoy,[2] Andrew Harvey,[1] Eoghan O'Malley,[1] Georg S Duesberg[2] and Jonathan N Coleman[1*]

[1] *School of Physics, CRANN & AMBER, Trinity College Dublin, Dublin 2, Ireland*

[2] *School of Chemistry, CRANN & AMBER, Trinity College Dublin, Dublin 2, Ireland*

*colemaj@tcd.ie

ABSTRACT: Here we demonstrate that the performance of catalytic electrodes, fabricated from liquid exfoliated MoS_2 nanosheets, can be optimized by maximizing the electrode thickness, coupled with the addition of carbon nanotubes. We find the current, and so the H_2 generation rate, at a given potential to increase linearly with electrode thickness to up ~5 μm after which saturation occurs. This linear increase is consistent with a simple model which allows a figure of merit to be extracted. The magnitude of this figure of merit implies that approximately two thirds of the possible catalytically active edge sites in this MoS_2 are inactive. We propose the saturation in current to be partly due to limitations associated with transporting charge through the resistive electrode to active sites. We resolve this by fabricating composite electrodes of MoS_2 nanosheets mixed with carbon nanotubes. We find both the electrode conductivity and the catalytic current at a given potential increase with nanotube content as described by percolation theory.

Keywords: Catalysis, edge, electrical resistance limited, active sites

ToC fig

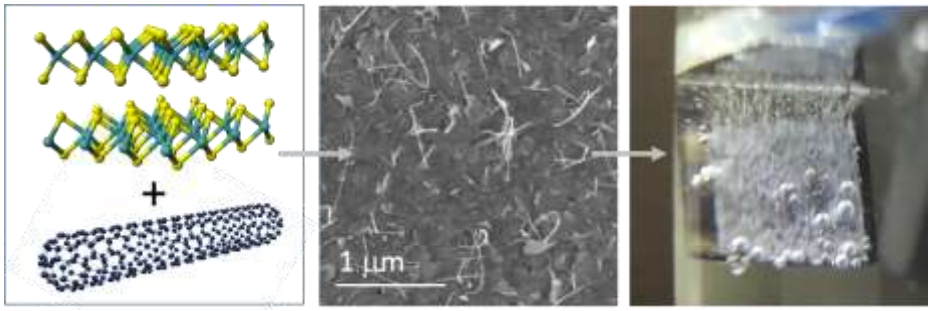

It is widely accepted that nanoscience has an important role to play in the next stages of development of energy generation and storage systems.[1] One example of this is the use of nanomaterials as catalysts for the generation of hydrogen for use as a fuel. This is generally achieved through the hydrogen evolution reaction (HER): $2H^+ + 2e^- \rightleftarrows H_2$. Currently, while platinum is the most efficient catalyst for the HER, its high price makes it far from the ideal material. To address this by replacing platinum will require the identification of a material which is abundant, non-toxic and cheap and of course can generate hydrogen at competitive rates at low applied potential. Finding a nanomaterial that can fulfill these requirements has generated much interest within the research community.[2-4]

In recent years, two dimensional (2D) nanomaterials such as transition metal dichalcogenides (TMDs) and transition metal oxides (TMOs) have shown great promise in a number of areas[5, 6] - including energy generation and storage.[7-11] In particular, exfoliated molybdenum disulfide (MoS_2) has received significant attention as a prospective HER electrocatalyst, with other TMDs such as $MoSe_2$, WS_2 and WSe_2 also showing potential.[3, 8, 12-15] MoS_2 is an earth-abundant layered material that can be exfoliated to give 2D nanosheets.[16] While MoS_2 is a poor HER catalyst in bulk form,[17, 18] exfoliated MoS_2 nanosheets (and other TMDs) are efficient HER catalysts. This has been demonstrated for thin films of liquid exfoliated MoS_2 nanosheets,[19-22] nanostructured MoS_2 particles[8, 18, 23] and MoS_2 grown on surfaces[24, 25] (although here the substrate has a significant impact[26]).

TMDs are most usually found in two polytypes: 2H-MoS_2 which is semiconducting and 1T-MoS_2 which is metallic.[5] The 2H form is most commonly encountered while the 1T polytype can be produced by lithium intercalation of 2H MoS_2. The HER activity of these polytypes is different: in the 1T form the basal plane is catalytically active[3] while in the 2H form the active sites are associated with uncoordinated disulphides at the nanosheet edge.[27-29]

High-quality 2D nanosheets can be produced quickly and easily using liquid phase exfoliation (LPE).[16, 30-33] This method is scalable[31] and gives dispersions of suspended MoS_2 nanosheets in a processable form. Importantly, advanced centrifugation and spectroscopic techniques can be used to control and measure the nanosheet thickness and size,[34] thus allowing for the selection of small nanosheets with greater numbers of edge sites. Nanosheet dispersions can easily be formed into porous films consisting of disordered arrays of nanosheets.[35] Such films have great potential for hydrogen evolution catalysis as their porous nature will facilitate access of the electrolyte throughout the interior of the electrode.[36] However, nanosheet catalysts are not perfect and require optimization. Probably the most

obvious route is to use the processability of LPE dispersions to optimize electrodes, for example by maximizing the number of catalytically active sites.

Increasing the density of active sites improves the performance while also reducing the catalytic footprint, thus reducing costs. A number of authors have approached this problem. Kong et al[12] and others[37-39] have grown films of vertically aligned MoS_2 nano-planes thereby maximizing the number of exposed edge sites. Reducing the particle size to optimize the ratio of edge to basal plane atoms has also proven effective.[40-45] Alternatively, introducing defects into the MoS_2 basal plane increases the number of active edge sites[41, 46] as has the use of amorphous instead of crystalline MoS_2.[47-51] Engineering the morphology of MoS_2 nanostructures to expose a high density of active edge sites such as single-crystal MoS_2 nanobelts,[52] nanotubes,[18] three dimensional MoS_2 spirals[53] or double-gyroid structures[54] is another effective method to improve HER activity.

A simple method for achieving highly active catalysts is to use thicker (*i.e.* higher nanosheet mass loading) electrodes to increase the overall number of available active sites.[21, 24, 39, 40, 43, 46, 48, 49, 51, 55-58] Thicker electrodes should improve activity so as long as electrolyte is free to move throughout the material (*i.e.* films are porous) and there is good electrical contact between the current collector and the active sites. However, increasing the nanosheet mass per area (M/A) of 2D catalytic electrodes has had limited success because, while the hydrogen production rate, as measured *via* the current flowing in the electrode, initially increases as the catalyst mass is increased, it invariably peaks at some loading level before falling off at higher M/A.[21, 24, 46, 48, 58] Unfortunately, this reduction often occurs at quite low mass loadings,[21, 24, 46, 48] limiting the performance of the catalyst. A detailed understanding of these limitations is lacking as a full analysis of the relationship between film thickness and activity has yet to be reported. Here, production of films from LPE nanosheets will be particularly advantageous as film formation using this method is particularly straightforward.[35]

There are a number of reasons why increasing the thickness of nanosheet films may not result in the desired performance increases. For example, for thick films mechanical robustness[35] may be a problem, leading to cracking – especially during gas evolution. Alternatively, in thick electrodes diffusion of ions into the interior will eventually limit the production rate, cancelling out any gains due to increased M/A. Perhaps even more significant are electrical limitations. For low conductivity electrode materials, performance will be limited by difficulties in getting electrons from the external circuit to catalytic sites. This is particularly likely to be the case in electrodes fabricated from semiconducting nanosheets such as MoS_2

which tend to give films with out-of-plane conductivity as low as ~10^{-9} S/m.[59] Such electrical limitations have been comprehensively documented for supercapacitor electrodes fabricated from MnO_2 nanosheets.[9]

As a result, while many papers in the literature report impressive data for thin film electrodes, the corresponding data for thick films is often not given. In fact it is quite uncommon to find nanosheet catalytic electrodes made with mass loading of 0.5 mg/cm^2 (*e.g.* ~1.7 μm for MoS_2) or higher. To achieve impressive performance for thicker films, reliable film formation methods must be used in parallel with efforts to improve the electrical properties of the electrodes. To address this, a number of approaches have been taken, such as supporting MoS_2 on carbon fibers,[60] graphene[19, 40, 50, 61-63] or carbon nanotubes.[57, 64-66] Alternatively a very successful approach has been to use lithium intercalation to transform the semiconducting 2H MoS_2 to the metallic 1T polytype.[20, 22, 43, 56, 67]

However, a simpler and perhaps more versatile approach to improve electrical properties of the electrode is to use liquid exfoliation coupled with solution mixing[35] to create dispersions of nanosheets mixed with carbon nanotubes. Such dispersions can be formed into robust composite films[35] which can be up to 10^9 times more conductive than a nanosheet networks alone[68] and also have improved mechanical properties.[9, 69] While this approach has been explored in detail for supercapacitor electrodes,[9] it has only been touched upon for electrocatalysis.[20, 48, 64] A full investigation of the effects of the addition of carbon nanotubes on the catalyst activity has not yet been attempted. Such a detailed study would be important both from the perspective of basic science and for practical reasons: *e.g.* to identify the minimum nanoconductor mass fraction required.

In this work we have used porous electrodes of randomly restacked MoS_2 nanosheets as a model system and investigated the enhancements in catalytic performance associated with maximizing electrode thickness. We show that the current density rises linearly with increasing thickness up to ~5 μm, much higher than previously shown in literature. Above ~5 μm, improvement in activity is shown to saturate with rising thickness, consistent with limitations associated with electrical conductivity. To combat this we fabricated composite films of MoS_2 nanosheets mixed with single-walled carbon nanotubes (SWNTs). We demonstrate that the addition of even a few weight percent of nanotubes can have dramatic effects on both the conductivity and the catalytic performance, with current density values more than doubling for the composite devices.

Results

MoS_2-only electrodes

Molybdenum disulphide (MoS_2) nanosheets were prepared by liquid phase exfoliation in aqueous surfactant solution using a combined process of sonication and centrifugation (see methods).[16] This process resulted in dark green dispersions of MoS_2 nanosheets in water, stabilized by the surfactant sodium cholate. TEM imaging (Figure 1A and B) confirmed the dispersed material to be in the form of thin nanosheets with statistical analysis (figure 1C) giving a mean flake length of L=114±4 nm. We also measured the average length/width aspect ratio to be k=1.98±0.09. The UV-vis extinction spectrum of such a dispersion is shown in figure 1D and is as expected for suspended few-layer 2H-MoS_2 nanosheets.[35] Using the measured extinction coefficient of ε_{345nm}=69 $mlmg^{-1}cm^{-1}$,[34] we found the MoS_2 concentration to be 0.6 mg/ml. As shown previously,[34] the ratio of extinction at the B-exciton to that at 345 nm is sensitive to the mean nanosheet length while the wavelength associated with the A-exciton is determined by the mean nanosheet thickness. Using previously identified metrics,[34] we analyze the extinction spectrum, finding the average flake length to be L=122±6 nm, in good agreement with the TEM data. In addition, we found the mean nanosheet thickness, expressed as the average number of layers per flake to be N=3.4±0.5.

The nanosheet dispersion was used to prepare thin films by vacuum filtration.[35] This method has the advantage that the deposited mass and resultant film thickness can be controlled relatively accurately. The films were prepared with mass per area (M/A) ranging from 0.06 – 4 mg/cm^2, a considerably broader range than used in previously published works.[40, 43, 46, 48, 56] A section of each film was then transferred onto conductive pyrolytic carbon (PyC) (figure 1E) using a transfer process outlined in the methods. SEM images were taken of the thick films, shown in figure 1F and G, revealing a highly porous structure consisting of a disordered array of MoS_2 nanosheets. Step profiles of each film were taken using a profilometer, giving a thickness range of 0.2 μm to 14 μm. The film density was found to be ρ_{film}~2890 kg/m^3, invariant with thickness, giving a film porosity of P~43% (taking the density of MoS_2 to be 5060 kg/m^3, see SI). This porosity is typical of that found for vacuum filtered nanosheet films.[70] This porous-network type morphology is advantageous for applications in electrocatalysis as it should enable free access of the electrolyte to the internal surface of the electrode. This should allow all active sites within the film to be exposed to electrolyte.

To test the electrocatalytic properties of such MoS_2 films with respect to the hydrogen evolution reaction, linear voltage sweeps (scan rate 5 mVs^{-1}) were performed on MoS_2 films

with thickness ranging from 0.2 μm to 14 μm (0.06 – 4 mg/cm^2). Typical polarization curves are presented in Figure 2A. It is immediately apparent that the thicker MoS_2 films have a dramatically increased current density and so greater HER activity compared to the thinner films. Much higher current densities were achieved for a given potential - as high as 44 mA/cm^2 for an 11.8 μm film compared to 3 mA/cm^2 for a 0.2 μm film (each measured at -0.4 V vs RHE). The onset potential (see figure 2A inset), defined here as the potential required to achieve J = 1 mA/cm^2, for a 0.2 μm thin film was observed to be -0.34 V vs RHE while an 11.8 μm film displayed the lowest onset potential of -0.116 V vs RHE which is one of the lowest onset potentials achieved in literature and comparable, if not superior to many similar and higher mass MoS_2 catalysts.[49, 55, 56] The origins of this improved HER activity can be attributed to the higher quantity of active MoS_2 edge sites available in the thicker films.

For a HER electrocatalyst, the relationship between the overpotential and the current density is described by the cathodic term of the Butler-Volmer equation, known as the Tafel equation, which can be written as:

$$J = -J_0 \times 10^{\eta/b} \quad (1)$$

where J is the measured current density, J_0 is the exchange current density, η is the overpotential, and b is the Tafel slope. Shown in figure 2B is our data for MoS_2 electrodes of different thicknesses plotted as η *versus* |J| on a Tafel plot. Values for b (and J_0) can be found by fitting the linear portion (*i.e*. at currents low enough to make mass transport limitations unimportant) of the Tafel plots to equation 1. We found the Tafel slopes of virtually all electrodes to be in the range 100-150 mV/decade with a mean of 125±17 mV/decade (see below for more detail).

The Tafel slope is a useful parameter and is a measure of the potential increase required to improve the current density by one order of magnitude. More fundamentally, analysis of the Tafel slope is used to evaluate the dominant HER mechanism at the electrode/electrolyte interface. It is generally accepted that the HER follows one of two possible reaction pathways.[71, 72] These pathways involve the Volmer reaction:

$$H_3O^+ + e^- + * \rightleftarrows H^* + H_2O \text{ (Volmer reaction)} \quad (2)$$

coupled with either the Heyrovsky or Tafel reactions:

$$H^* + H_3O^+ + e^- \rightleftarrows H_2 + H_2O + * \text{ (Heyrovsky reaction)} \quad (3)$$

$$H^* + H^* \rightleftarrows H_2 + 2* \text{ (Tafel reaction)} \quad (4)$$

to give either the Volmer-Heyrovsky or Volmer-Tafel mechanism. In equations 2-4, * indicates the catalytic active site. Either the first (equation 2) or second (equations 3 or 4) reaction step in the mechanism is the rate determining step, r.d.s, of the reaction. According to Conway[71] the dominating mechanism will depend on the surface coverage of adsorbed hydrogen, H_{ads}, on the electrode. For the case of high surface coverage a Tafel slope of 40 mV/dec or 30 mV/dec suggests the Heyrovsky or Tafel reaction dominates. When surface coverage of H_{ads} is relatively low the Volmer reaction dominates and a Tafel slope of 120 mV/dec is observed. While the measured value of 125±17 mV/dec implies the rate limiting step to be the Volmer reaction in our case, it is worth exploring if this is the case independent of electrode thickness.

Dependence of Hydrogen evolution with electrode thickness

To do this, we found the Tafel slope for each film which we plotted against film thickness, as shown in figure 3A. The Tafel slope remains relatively constant with film thickness, (<b>=125±17 mV/dec), indicating the Volmer reaction to be the r.d.s of our MoS_2 catalyst for all film thicknesses studied. This agrees with many papers in the literature which give Tafel slopes between 100 – 145 mV/dec for 2H MoS_2.[12, 18, 22, 42-44, 56, 58, 73, 74] Interestingly Vrubel et al[48] reported an increase in Tafel slope with higher mass loading of amorphous MoS_3 dropcast onto glassy carbon electrodes (from 41 mV/dec for 8 μg/cm^2 to 63 mV/dec for 128 μg/cm^2). They attribute the increase to decreased efficiency in electron and proton transfer with the higher loading films. It is worth noting that, when considering all types of nanostructured MoS_2 an even larger spread of Tafel slopes is found, ranging from as low as 40 mV/dec (often 1T MoS_2) up to 185 mV/dec.[12, 18, 22, 28, 40-44, 48, 55, 56, 58, 61, 73-76] It appears the Tafel slope can vary greatly for different preparations of the same material. In addition, Kong et al[12] noted that substrate morphology significantly affects the Tafel slope. The same MoS_2 made on smooth glassy carbon, rough glassy carbon or Mo foil gave Tafel slopes of 105-120, 86 and 75 mV/dec respectfully. It seems there is a lack of sufficient understanding of the critical factors influencing the Tafel slope of MoS_2 electrocatalysts,[18] making materials comparison difficult.

Increasing the film thickness increases the number of available catalytic sites within the interior of the film. This implies that both the exchange current density, J_0, and the current at a given potential, $J(V)$ should scale directly with film thickness. Figure 3B shows J_0 to increase with film thickness from ~0.003 mA/cm^2 for a 0.76 μm film to an impressive ~0.13 mA/cm^2 at a thickness of 11.4 μm. This is one of the highest values of exchange current density in literature with only 1T MoS_2 achieving higher current values.[43, 56] Although, as is often the case for J_0, the data is scattered, it is clearly linear (dashed line) with a slope of

dJ_0/dt=0.018±0.003 mAcm^{-2}μm^{-1} (equivalent to a current per electrode volume of 180±30 kA/m^3).

It is also useful to consider the current at a given potential as a measure of the effectiveness of the electrode as a HER catalyst. Figure 3C shows the positive value of the current density at V= -250 mV vs RHE, $-J_{-250\text{mV}}$, plotted *versus* electrode thickness. Here the data is much less scattered and clearly scales linearly with electrode thickness ($d(-J_{-250mV})/dt$ =1.2 mAcm^{-2}μm^{-1}) as far as t ~5 μm, after which the current saturates. As long as the electrode morphology is thickness independent, the number (per unit area) of active sites will increase linearly with electrode thicknesses. Then, assuming the electrolyte is free to permeate throughout the entire film and there is nothing limiting the transport of charge from the current collector to the active sites, a linear increase in current with thickness implies that Hydrogen generation is occurring throughout the internal free volume of the electrode. This is an important result as it shows that in porous electrodes such as these, the gas production rate can be increased simply by increasing the electrode mass.

We can understand the thickness dependence of the current density quantitatively by developing a simple model which is based on the linear relationship between the current and the hydrogen production rate.[77] Assuming all active sites on the internal surface of the electrode are in contact with the electrolyte, that the evolved gas can escape and that nothing limits current flow between the external circuit and the catalytic sites, we can write the current density as

$$J = -neN_s R / A \qquad (5)$$

where N_s is the number of active sites, R is the number of H_2 molecules produced per site per second (the turnover number), A is the geometric area of the electrode and n is the number of electrons supplied per molecule produced (N.B. n=2 for HER but this equation can be adapted for other reactions by changing n).

For 2H-MoS_2, the catalytic sites are associated with edge sulphurs.[18, 27-29] However, only a fraction of these may be active, perhaps due to functionalization with impurity species.[27, 28] Thus we characterise the active sites solely *via* their location on the nanosheet edge and through their separation, which we express *via* the number of catalytic active sites per unit monolayer edge length, B. Thus, in a few-layer nanosheet, the number of active sites is B times the perimeter length times the number of monomers per nanosheet. We can work out the total number of active sites by further multiplying by the number of nanosheets per unit mass times the electrode mass, M. Then we find:

$$N_s = \frac{2B(1+k)}{\rho_{NS} L d_0} M \quad (6)$$

where L is the mean nanosheet length, k is the mean nanosheet length/width aspect ratio (given above), d_0=0.6 nm is the monomer thickness and ρ_{NS} is the nanosheet density (5060 kg/m^3 for MoS_2). Combining equations 5 and 6, we find

$$J = -neR \frac{2B(1+k)}{\rho_{NS} L d_0} \frac{M}{A} \quad (7a)$$

Alternatively, this can be written as a function of electrode thickness, t:

$$J = -2ne[RB]\left[\frac{(1+k)(1-P)}{L d_0}\right] t \quad (7b)$$

where P is the porosity ($P = 1 - \rho_{Film} / \rho_{NS}$).

Based on the Butler-Volmer equation, the turnover number should depend on overpotential as $R = R_0 \times 10^{\eta/b}$, where R_0 is the turnover number at zero overpotential, allowing us to write

$$J = -2ne[R_0 B] \times 10^{\eta/b} \times \left[\frac{(1+k)(1-P)}{L d_0}\right] t \quad (8)$$

This equation completely describes the thickness dependence observed in figure 3C. By comparison with equation 1, this means we can write the exchange current density as

$$J_0 = 2ne[R_0 B]\left[\frac{(1+k)(1-P)}{L d_0}\right] t \quad (9)$$

We note that the first square bracketed quantity is a measure of the catalytic properties of the nanosheets while the second square bracketed property depends on the nanosheet dimensions and film morphology. As these second set of properties are known, we can use the fit from figure 3B to find $R_0 B \approx 11 \pm 2.5$ H_2 molecules s^{-1} μm^{-1} of monolayer edge length. We propose that this number is a figure of merit which can be used to compare the catalytic performance of different 2D materials.

In general, most papers quote R_0 or $R(\eta)$ as a figure of merit for the nanosheet catalytic activity. However, this is not strictly correct as these parameters describe the activity of the catalytic site. The overall activity of the nanosheet is better labelled by R_0B as it describes both the site activity and the site density. In fact, disentangling these parameters is always problematic as it can be hard to accurately measure B (or more generally the site density). In

fact, many papers quote values of R_0 or $R(\eta)$ which are calculated using values of B which are based on dubious assumptions or approximations. Here we take a different approach. The catalytically active sites are edge disulphides[27-29] which are 0.32 nm apart[78] and only exist on the S-rich edge which accounts for half the total edge length on average. Not all of these sites will be active as some may have become functionalised during the exfoliation process. Using this information, we find that B_{max}=1.56 nm^{-1} is the maximum possible number of active sites per edge length. Given that we have measured $R_0 B \approx 11 \pm 2.5$ H_2 molecules s^{-1} μm^{-1}, this means that $R_{0,min}$~(64±15)×10^{-3} s^{-1} is the minimum zero-overpotential turnover frequency consistent with our data. This is certainly in line with most of the data in the literature for 2H-MoS_2.[12, 46, 47, 64, 79] If we take the zero-overpotential turnover frequency of R_0=0.02 s^{-1}, quoted for perfect MoS_2 edges by Jaramillo,[28] this means our MoS_2 is consistent with B=0.55±0.013 nm^{-1}. Comparing this value to B_{max} implies that approximately two out of every three disulphides in our LPE MoS_2 are inactive. This in turn implies that the performance of LPE MoS_2 quoted here could possibly be tripled by chemically treating the edges to activate all disulphides. This is of course in addition, to more obvious strategies such as reducing nanosheet length[42, 60, 80] or increasing the aspect ratio[52] implied by equation 9.

It is worth considering what could possibly be achieved by optimising the performance of LPE MoS_2 electrodes. Assuming chemical treatment could render all edge disulphide groups active (*i.e.* yielding B=1.56 nm^{-1}), and that the exfoliation could be modified to give nanosheets with aspect ratio of 4 and then performing size selection[34] to reduce the nanosheet length to 5 nm on average[45] would give a value of dJ_0/dt=19 MA/m^3, almost two orders of magnitude greater than achieved here.

We can also plot the potential required to generate a given current density (here 3 mA/cm^2) *versus* electrode thickness as shown in figure 3D (plotted as $-V_{3mA/cm2}$). We find a logarithmic decrease from ~400 mV at t ~200 nm to ~200 mV for t~5-6 μm, after which the potential saturates. We can understand this *via* the linearity of J_0 with t embodied in eq 9. With this in mind, we can rewrite equation 1 as $|J| = dJ_0/dt \times t \times 10^{\eta/b}$. Then, the overpotential for a given current is given by

$$\eta(J) = -b\log t + b\log\left(\frac{|J|}{dJ_0/dt}\right) \qquad (10)$$

This equation implies that the slope of an $\eta(J)$ *versus* $\log(t)$ graph should be equal to the Tafel slope of the nanosheets. This is supported by the fact that the slope of the dashed fit line in figure 3D is 129 mV/dec, very close to the mean Tafel slope of 125 mV/dec found above.

It is worth considering how the material optimisation described above would affect the potential required to achieve a given current, say -30 mA/cm^2. Using equation 10 and assuming a Tafel slope of b=125 mV/dec, a thickness of 5 μm and an optimised value of dJ_0/dt=19 MA/m^3 we find that $\eta(J$=-30 mA/cm^2)=63 mV. This would be an extremely low potential and would render LPE MoS_2 extremely attractive as a HER catalyst.

The improvements in both $|J|$ and $\eta(J)$ with thickness shown in figures 3C and D begin to saturate at thicknesses above t~5 μm (M/A=1.44 mg/cm^2). This can be seen more clearly in the inset in figure 3C which shows the current density divided by electrode thickness ($-J_{-250mV}/t$) plotted *versus* electrode thickness. While $-J_{-250mV}/t$ is roughly constant at ~1.2×10^7 A/m^3 for low electrode thickness's, it clearly falls off for larger thicknesses. Others in the literature have also reported a degradation in performance when increasing the mass loading of their films.[21, 24, 46, 48, 58] However, it should be noted that all of these M/A limits are far lower than for our electrodes. As described above, there are a number of reasons why performance should fall off as the electrode thickness increases, namely diffusion, mechanical and electrical limitations. We believe that the latter two problems can be addressed relatively simply by adding nanotubes to the electrode.

Composite films of MoS_2 and SWNTs

As demonstrated recently for MnO_2 nanosheet supercapacitors,[9] a simple solution to the electrical transport issues of the thicker films is to mix single-walled carbon nanotubes (SWNT) with the nanosheets to form a hybrid film. The nanotubes will form a conductive network throughout the film, facilitating charge transport from the current collector to the active edge sites. This work[9] showed that just a few volume percent nanotubes could lead to a dramatic enhancement in both the electrical and capacitance properties of MnO_2 supercapacitors. Notably, these enhancements were both fully consistent with percolation theory.

To insure a minimum amount of non-active material is added a full characterisation of SWNT loading is needed. We prepared a range of mixed dispersions of MoS_2/SWNTs by solution mixing (see methods). These were filtered to form composite films which were then

transferred onto PyC electrodes as before. To facilitate analysis, the composite films had a fixed MoS_2 mass of ~1.45 mg/cm^2 (~5.05 μm) while the SWNT mass fraction, M_f, was varied from 0.03 – 13 wt% ($M_f = M_{cnt}/(M_{cnt}+M_{MoS2})$).

We performed SEM analysis of the composite films with a typical example shown in figure 4A (top left inset, M_f=13 wt%). The SWNTs are clearly visible suggesting effective mixing of the SWNTs within the MoS_2 matrix. The composite films were also found to maintain their high porosity, with free volume of ~45±5% (see SI), unchanged relative to MoS_2-only films. This is important as it shows that any improvements associated with addition of SWNTs are not due to increasing porosity or morphological changes.

We propose that addition of nanotubes will facilitate the transport of electrons from the current collector to the catalytically active sites within the electrode. This will require the enhancement of the out of plane conductivity of the electrode. However, for reasons of practicality, we assess the effect of the nanotubes by measuring the in-plane conductivities, σ, for a range of MoS_2/SWNT composites. Compared to the known in-plane conductivity of an MoS_2 nanosheet network (~10^{-6} S/m, ref[68, 81]), the composites showed dramatically increased conductivity. As shown in figure 4A, σ increases rapidly with M_f, reaching ~275 S/m for M_f =1 wt% and ~1.2×10^4 S/m for the M_f =13 wt%. This behaviour is consistent with previously reported composites of carbon nanotubes mixed with MoS_2 nansosheets,[68] as well as the broader field of nanotube-filled polymers.[82]

The electrical properties of insulating matrices filled with conducting particles are usually described using percolation theory.[83] Within this framework, as the filler volume fraction (ϕ) is increased, the film conductivity remains similar to that of the matrix until a critical filler volume fraction, the percolation threshold, $\phi_{c,e}$, is reached. At this point the first conducting path across the film is formed and current begins to flow. Above the percolation threshold, the conductivity is described by the percolation scaling law:[68, 82, 83]

$$\sigma = \sigma_0(\phi - \phi_{c,e})^n \qquad (11)$$

where n is the percolation exponent and σ_0 approximates the conductivity of film prepared from filler particles alone. As shown in figure 4A (bottom right inset), our data is consistent with percolation theory, with fitting giving values of σ_0=1×10^5 S/m, $\phi_{c,e}$=0.5 vol% and n=1.3. This value of σ_0 is consistent with other percolation studies,[9, 68] but also with measurements on nanotubes films showing conductivities of ~10^5 S/m are generally achieved.[84] The percolation threshold is also as expected[9, 68] and is consistent with theory which predicts $\phi_{c,e}$ to be

approximately given by the ratio of mean nanotube diameter to length.[82] Such a small percolation threshold for conductivity is advantageous as only a very small amount of SWNT filler is required for a large increase in conductivity. This means very little catalytic material has to be sacrificed to introduce the conductive paths. Finally the exponent is identical to the universal percolation exponent (n=1.3) for transport in two dimensions and similar to measured percolation exponents (n=1.2 and n=1.8) in other nanotube-nanosheet networks.[9, 68]

It is important to point out that the paragraphs above describe in-plane conductivity whereas it is the out-of-plane conductivity that is relevant in HER. This distinction is important as MoS_2 films are known to be electrically anisotropic with out-of-plane conductivity ~1000 times lower than in-plane conductivity.[59, 81] To our knowledge the out-of-plane conductivity has never been measured for nanosheet-nanotube composites partly due to the difficulty in avoiding pinholes. However, it is reasonable to assume that addition of nanotubes will result in out-of-plane conductivity increases which are in proportion to the measured in-plane increases described above. This hypothesis is supported by the large increases in supercapacitance of MnO_2 nanosheet films recently observed on addition of nanotubes.[9] Such increases could not occur if addition of nanotubes did not enhance the out-of-plane conductivity.

HER measurements for MoS_2/SWNT films

We have shown that small amounts of added SWNTs can dramatically improve the DC conductivity of thick MoS_2 films. The next step is to examine whether this added conductive value plays a role in improving the actual catalytic performance of the thick MoS_2 electrodes. To do this we performed linear voltage sweep measurements on a series of composites (MoS_2 M/A=1.45 mg/cm^2, t~5 μm) and plotted polarisation curves shown in figure 4B. A considerable increase in current density is measured with the addition of just a few wt% SWNTs. This strongly supports the idea that the introduction of conductive paths facilitates charge transport to active sites of the MoS_2. The onset potential is also reduced from -0.140V vs RHE to -0.112 V vs RHE for a film of just 10 wt% SWNTs. The addition of SWNTs clearly has a positive impact on the HER catalytic activity

Tafel plots were then generated for each composite film (figure 4B inset) and the Tafel slopes extracted. Figure 5A shows the Tafel slope remains roughly constant, around 102±17 mV/dec, when plotted against SWNT volume fraction. The invariance of Tafel slope with the addition of SWNTs suggests that while the charge transport properties have improved the

reaction is still limited by the inefficient adsorption of H^+. From investigation of the literature there does not seem to be a consensus on the effect of adding carbon nanotubes to the Tafel slope. Vrubel et al[48] and Dai et al[64] noticed a decrease in Tafel slope with the addition of MWNTs, however Voiry et al[20] observed an increase when adding SWNTs.

We also performed electrochemical impedance spectroscopy on an MoS_2-only electrode and a number of composite electrodes with varying nanotube content (all ~5 µm thickness). Data for a subset of electrodes is plotted in figure 4C as Nyquist plots. While all curves can be fitted to a model[85] which describes both the MoS_2/SWNT electrode and interfacial processes (see SI), the main effect of adding nanotubes is to reduce the charge transfer resistance (see below).

In order to further characterise the impact of adding nanotubes to the MoS_2 electrode, we have plotted J_0, $-J_{-250mV}$ and $-V_{-3mA/cm2}$ *versus* SWNT volume fraction in figures 5B-D. Shown in figure 5B is data for exchange current density, J_0, as a function of nanotube volume fraction. Here the data is somewhat scattered as is often the case for values of J_0 extracted from Tafel plots. However, the dashed line is a guide to the eye and suggests the exchange current does indeed increase with nanotube content.

More reliable is data for current density read directly from polarisation curves. Shown in figure 5C is data for the current density, measured at V=-250 mV vs RHE, plotted *versus* ϕ. It is clear from this data that the current is constant at 7-8 mA/cm^2 at low volume fractions but increases sharply when the volume fraction surpasses 0.5-1 vol%, reaching ~14 mA/cm^2 for nanotube contents of ~20 vol%. We interpret this behaviour as reflecting the improved charge transport through the film above the percolation threshold. This facilitates efficient delivery of electrons to the catalytically active sites and results in higher hydrogen production rates. Similar behaviour has been seen previously for MnO_2/SWNT supercapacitors[9] and MoS_2/SWNT lithium ion battery electrodes.[86] In the case of the composite supercapacitors, it was found that the excess capacitance, *i.e.* the capacitance increase relative to the matrix associated with the addition of the nanotubes followed a percolation scaling law.[9]

Assuming the same behaviour is found here would imply the hydrogen production rate, and so the current density to scale as

$$-J_{-250mV} = -J_{-250mV}^{MoS2} + J_{Perc}\left(\phi - \phi_{c,c}\right)^{n_c} \qquad (12a)$$

where J_{-250mV}^{MoS2} is the current density at -250 mV for an MoS_2 only film, J_{Perc} is a constant and $\phi_{\mathrm{c,c}}$ and n_{c} are the percolation threshold and exponent associated with the percolation of

catalysis. We have fit equation 12a to the current density *versus* ϕ data in figure 5C, finding very good agreement. Shown in figure 5D is the percolation plot where we fit the data to:

$$\left|\Delta J\right|_{-250mV} = J_{Perc}\left(\phi - \phi_{c,c}\right)^{n_c} \qquad (12b)$$

where $\left|\Delta J\right|_{-250mV} = -(J_{-250mV} - J_{-250mV}^{MoS_2})$ and $\left(\phi - \phi_{c,c}\right)$ is the known as reduced volume fraction. This graph shows particularly clearly that this data is consistent with percolation theory. From the fitting, we find values of $\phi_{c,c}$=0.5 vol% and n_c=0.75. Interestingly, the catalytic percolation threshold is identical to the electrical percolation threshold, strongly suggesting the performance increase to be associated with the conductivity increase. The catalytic percolation exponent is significantly smaller than the electrical percolation exponent as observed previously for MnO_2/SWNT composite supercapacitors[9] and MoS_2/SWNT composite Li ion battery electrodes.[87] While this is not fully understood, we suggest that the percolative nature of the hydrogen production rate is due to the scaling of the extent of the nanotube network with ϕ. When $\phi > \phi_c$, nanotubes can either belong to the network spanning the entire film or be isolated from it. The strength of the network is the probability that a given nanotube belongs to the network and is given by $P \propto (\phi - \phi_c)^{\beta}$.[83] We propose that stronger networks are more able to deliver electrons to catalytic sites throughout the film. This results in the power law scaling of $-J_{-250mV}$ with $\phi - \phi_c$. That the exponent is relatively low may be a reflection of the fact that β is usually quite low; values as low as 0.14 have been proposed for certain lattices.[88] However, we note that we would not expect the exponent n_c to be equal to β. It is likely that the exact value of n_c is specific to the details of the parameter being examined (*i.e.* here $-J_{-250mV}$).

Another important parameter is the potential required to achieve a given current density. When continuously producing hydrogen at a constant rate, it is critical that the required potential is as low as possible to minimise power consumption. Shown in figure 5E is a graph of the potential required to generate a current density of -3 mA/cm^2 plotted *versus* SWNT volume fraction. At low volume fractions, the potential is similar to but slightly lower than the equivalent potential in MoS_2 only films. However at ~0.7 vol% the potential begins to fall sharply, reaching 170 mV for a nanotube content of 13 vol%. Because the power consumption in a hydrogen generator will scale as $P \propto JV$ and because the hydrogen production rate scales linearly with *J*, this reduction in $V_{-3mA/cm2}$, is equivalent to a 15% reduction in the energy cost per H_2 molecule relative to a MoS_2 only electrode of equivalent thickness.

Another parameter which is important for the description of the HER is the charge transfer resistance, R_{ct}. This resistance essentially describes the rate of charge transfer across the electrode/electrolyte during the Volmer or Heyrovsky reactions. We found R_{ct} (when multiplied by geometric electrode area) to be 130 Ωcm^2 for the MoS_2-only electrode. However, the charge transfer resistance fell sharply on addition of carbon nanotubes, reaching 72 Ωcm^2 for the 0.14 vol% sample. We suggest that the presence of nanotubes increases the conductivity of the electrode and so enables a rapid supply of electrones from current collector to catalytic sites. This allows electron transfer to approach its intrinsic rate and results in a reduction of R_{ct}.

Finally, we have measured the stability of electrodes fabricated from both MoS_2 nanosheets and a 14 vol% MoS_2/SWNT composite (t=5 μm in both cases). We performed chronoamperometry at a fixed overpotential of 300 mV for approximately 160 minutes on each electrode (see SI). In both cases, we found a steady fall in current density over the first hour with subsequent stabilisation of current. We find a 48% fall off in current for the MoS_2-only sample over approximately two and a half hours. However, addition of 10% nanotubes significantly stabilized the electrode with a fall-off of only 27% over the same timescale. We suggest that the source of instability is the mechanical fragmentation of the electrode due to the stresses associated with bubble release. As observed previously,[35] addition of nanotubes should significantly increase the robustness of the electrode resulting in the observed increase in stability.

Conclusions

We have demonstrated that dispersions of liquid exfoliated nanosheets are a versatile starting material for the production of electrodes for catalysing the hydrogen evolution reaction. Such electrodes can easily be fabricated at controlled thicknesses up to ~10 μm. We found the Tafel slope to be independent of electrode thickness, consistent with the hydrogen production rate being limited by the Volmer reaction. The exchange current density and the current density at fixed potential scaled linearly with electrode thickness while the potential required to generate a given current fell logarithmically with thickness. These behaviours imply that the electrolyte penetrates throughout the porous internal surface of the electrode resulting in hydrogen production at all available active sites. However, this behaviour only persists up to thicknesses of ~5 μm. For thicker electrodes, the current and potential saturates with no further gains achievable by increasing electrode thickness.

This saturation is partly due to the difficulties of transporting charge through a thick insulating film, coupled with the reduction in mechanical robustness as the thickness is

increased. We addressed this by adding carbon nanotubes to the electrode, increasing both its electrical and mechanical properties. While the Tafel slope was largely independent of nanotube content, we found the exchange current density, the current density at fixed potential and the potential required to generate a given current to improve with the increasing nanotube content. This increase in performance is associated with the introduction of conducting paths to the thick electrodes allowing for charge to better reach previously inaccessible sites. This activates more of the MoS_2 thus leading to a more active catalyst. This is further supporting evidence to suggest that the saturation of electrode performance at higher thicknesses is majorly due to electrical and not mass transport limitations. Interestingly, we found the current at a given potential to be well described by percolation theory.

While we have used MoS_2 as an electrocatalyst for the hydrogen evolution reaction as a model system to study the effect of thickness and nanotube content, we believe the learnings are general and could be applied to other systems such as $Ni(OH)_2$ for catalysis of the oxygen reduction reaction. We believe that the strategies outlined here may be enough to push another system across the boundary from promising to state of the art and demonstrate the usefulness of nanomaterials science to fields such as catalysis.

Methods

Preparation of MoS_2 dispersions:

Stock solutions of sodium cholate (SC, Sigma-Aldrich) were prepared by adding deionised water at SC concentrations of 12 mg/ml and 3 mg/ml. MoS_2 powder (MoS_2, Sigma-Aldrich) was added to 80 ml of the 12 mg/ml SC solution at a concentration of 30 mg/ml and exfoliated using a high power sonic tip (VibraCell CVX; 750 W, 60 kHz) for 1 hour at 60% amplitude, pulse rate 6 s on 2 s off. The formed dispersion was immediately centrifuged (Heraeus Multifuge X1) at 5500 rpm for 99 min and the supernatant, containing very small nanoparticles and impurities, was removed. The sediment was redispersed in the solution of 3 mg/ml sodium cholate to a volume of 80 ml and sonicated for 8 hours at 60% amplitude, pulse rate 4 s on 4 s off, to finish the exfoliation process. The dispersion was then let sit for 2 hours to allow large aggregates to settle.

Control over the average flakes size of the dispersion was possible using precise centrifugation conditions. The dispersion was first centrifuged at 5000 rpm for 2.5 hours and the supernatant, containing very small flakes, was removed and discarded. The sediment was redispersed in the 3 mg/ml SC solution and centrifuged at 2000 rpm for 2.5 hours. This step

separates out larger flakes form the desired flake size. The supernatant was retrieved and formed a stable dispersion. The concentration of exfoliated MoS_2 was determined by UV-visible absorption spectroscopy at wavelength of 345 nm using a Varian Cary 6000i. Using the Beer-Lambert relation: $C = A/\varepsilon l$, the dispersion concentration, C, was found, using an extinction coefficient, of ε_{345nm}=69 $mlmg^{-1}cm^{-1}$,[34] and a cell length, *l*=1 cm. The average flake length and number of layers per flake of the exfoliated MoS_2 was then calculated from the absorption spectrum using previously reported metrics.[34]

Preparation of SWNT dispersions:

A stock solution of 10 mg/ml SC in deionised water was prepared. Single-walled carbon nanotube powder (SWNTs, arc-discharge, Iljin Nanotech Co.) was added to the solution such that the SC/SWNT mass ratio in the resulting dispersion was 10:1 (SWNT concentration 1 mg/ml). The dispersion was then divided into 10 ml vials and each vial received 5 min of high power tip sonication at 25% amplitude, 2 s on 2 s off, then 30 mins in a sonic bath (Branson 1510-MT sonic bath, 20kHz), followed by another 5 min of tip sonication. The dispersions were then centrifuged at 5500 rpm for 90 min. The supernatant of each dispersion was retrieved. The concentration of the resulting dispersion was found by measuring the absorption at 660 nm and using the extinction coefficient of SWNTs, 3389 $mlmg^{-1}m^{-1}$.

Film formation and device preparation

Dispersions of MoS_2 in SC were vacuum filtered through porous mixed cellulose ester filter membranes (MF-Milipore membrane, hydrophilic, 0.025 um pore size, 47 mm diameter). Precise control over the mass per unit area (M/A) of filtered material was achieved by filtering known volumes of a dispersion with known concentration. This resulted in spatially uniform films ranging in M/A.

To make composite films of MoS_2 and SWNTs, filtering smaller volumes (preferably <5 ml) was found to give better results. This reduced the filtering time and resulted in a more even distribution of SWNTs throughout the MoS_2 matrix. To achieve a high concentration of dispersed MoS_2, select volumes of known mass were centrifuged at 16000 rpm for 2.5 hours. This resulted in the MoS_2 being sedimented out of solution. The excess liquid was removed and the sediment was redispersed in a smaller volume of 3 mg/ml SC. An amount of SWNT dispersion was then added to the MoS_2 dispersion, with the precise volume dependent on the

mass ratio needed, and put into the sonic bath for 30 min. Films were then made by vacuum filtration.

To remove the remaining surfactant, both MoS_2-only and composite films were washed by filtering 200 ml of deionised water through the porous films. The resulting films (diameter 36 mm) were left to dry overnight. Once dry, they were cut to the desired dimensions and transferred to a pyrolytic carbon (PyC) or glass substrates for electrochemical testing, SEM imaging, profilometry thickness and electrical measurements. The cellulose membrane was removed by applying pressure to the film, wetting it with acetone vapour and subjecting it to a series of acetone baths. The acetone dissolves the cellulose membrane and leaves the films behind on the substrate surface (see for example ref [84]). Pyrolytic carbon was grown by chemical vapour deposition (CVD) as described previously.[89]

Electrode Characterisation:

Film thickness was measured using a Dektak 6M, Veeco Instruments profilometer. Step profiles were taken at four different locations to get an average film thickness for each electrode. Films ranged in thickness from 0.2 μm to 14 μm. This is a non-destructive process and allows for the film thickness to be obtained for each electrode before electrochemical measurements. For composites, the nanotube mass fraction, M_f, was converted to volume fraction, ϕ, using $\phi = V_{NT} / V_T = M_f \rho_{film} / \rho_{NT}$ where V_{NT} and V_T are the volumes occupied by nanotubes and entire film respectively and ρ_{Film} and ρ_{NT} are the densities of the film and the nanotubes respectively (ρ_{NT}=1800 kg/m^3). Electrical conductivity measurements were made with a Keithley 2400 source meter (Keithley Instruments, Inc) using a four probe technique. Silver wire contacts were bonded to the film using Agar Scientific silver paint and electrode spacing was carefully recorded using ImageJ software. SEM images were obtained using a ZEISS Ultra Plus (Carl Zeiss Group), 2 kV accelerating voltage, 30 μm aperture and a working distance of approximately 1-2 mm. The samples were loaded onto the SEM stub using sticky carbon tape.

Electrochemical measurements were then carried out to evaluate the performance of the thick MoS_2 and MoS_2/SWNT composites as catalysts for the HER. Films were cut to an area of 0.64 cm^2 and transferred onto a PyC substrate. Electrochemical measurements were performed in a three-electrode electrochemical cell in 0.5 M H_2SO_4 acidic electrolyte, with a large graphite counter electrode and a reversible hydrogen electrode (RHE) as the reference electrode. Catalytic activity was measured by performing Linear Sweep Voltammetry (LSV)

and Electrochemical Impedance Spectroscopy (EIS) with a Gamry Reference 3000 potentiostat at an overpotential of 150 mV. Samples were conditioned at a given voltage before each test. Linear voltage sweeps were performed at a scan rate of 5 mVs^{-1} in a window from 0 V to -0.6 V (vs RHE). The equivalent series resistance (R_{ESR}) of the system was determined by impedance spectroscopy (EIS) in the frequency range of 0.1 to 10 mHz with perturbation voltage amplitude of 10 mV. All the data was corrected for the electrolyte resistance by iR compensation.

Supporting information

Density and porosity data, stability data, impedance fitting information.

Acknowledgement

This work was predominantly funded by Science Foundation Ireland (11/PI/1087) as well as the European Research Council (SEMANTICS). The research leading to these results has also received funding from the European Union Seventh Framework Programme under grant agreement n°604391 Graphene Flagship and the Science Foundation Ireland (SFI) funded centre AMBER (SFI/12/RC/2278**).** NMcE acknowledges SFI for 14/TIDA/2329.

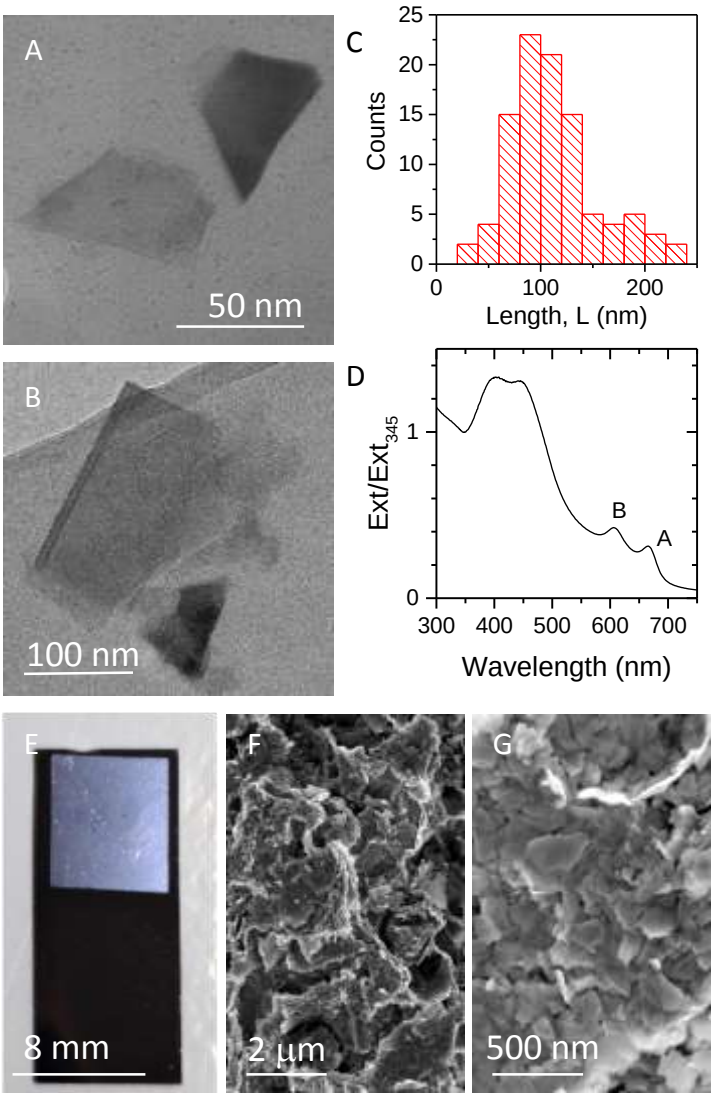

Figure 1: Characterization of MoS_2 nanosheets. (A and B) TEM images of exfoliated MoS_2 nanoflakes. (C) Histogram of flake length distribution. Average exfoliated flake size was L=114±4 nm. (D) Optical extinction of an MoS_2 nanosheet dispersion. The A- and B-excitons are indicated. (E) Catalytic electrode fabricated from deposited MoS_2 flakes on a pyrolytic carbon substrate. (F-G) SEM images of (E) a 9 μm thick MoS_2 film and (F) magnified image of the same film, showing the porous structure of the film.

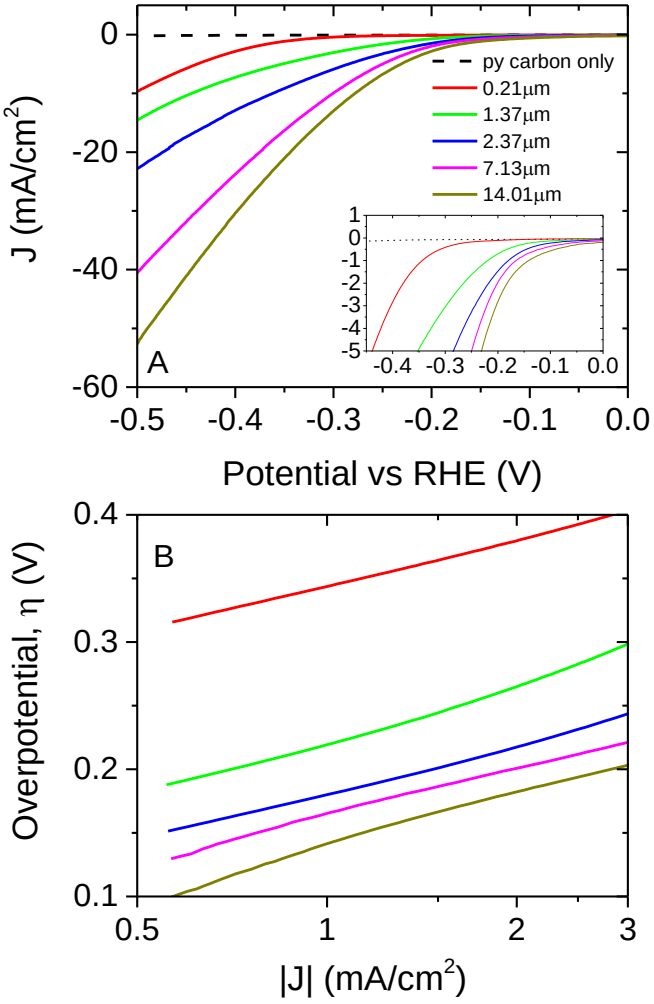

Figure 2: (A) Polarization curves (inset: lower potential regime) measured for MoS_2-only films ranging in thickness from 0.21 μm to 14 μm. Thicker films show much higher current densities for the same potential values and much lower onset potentials. (B) Corresponding Tafel plots.

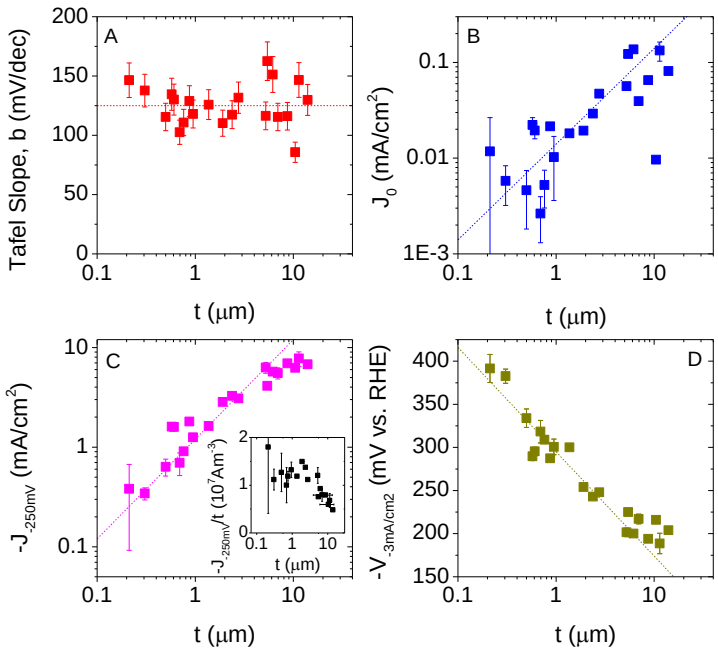

Figure 3: Relationship between electrocatalytic performance and thickness of MoS_2 only films. (A) Tafel slope *versus* MoS_2 film thickness. There is no significant change in Tafel slope with increasing film thickness, with average slope of b~125±17 mV/dec (B) Exchange current density *versus* MoS_2 film thickness showing linear increase of J_0 with rising thickness. (C) Current density measured at a potential of -250 mV vs RHE plotted *versus* MoS_2 film thickness. Current increases linearly (dashed line) with film thickness up to ~5 μm then begins to saturate. Inset: Current density normalised to electrode thickness which shows a steady fall off with thickness. (D) Potential required to achieve a current density of -3 mA/cm^2 plotted *versus* MoS_2 film thickness. The dashed line represents a logarithmic decrease.

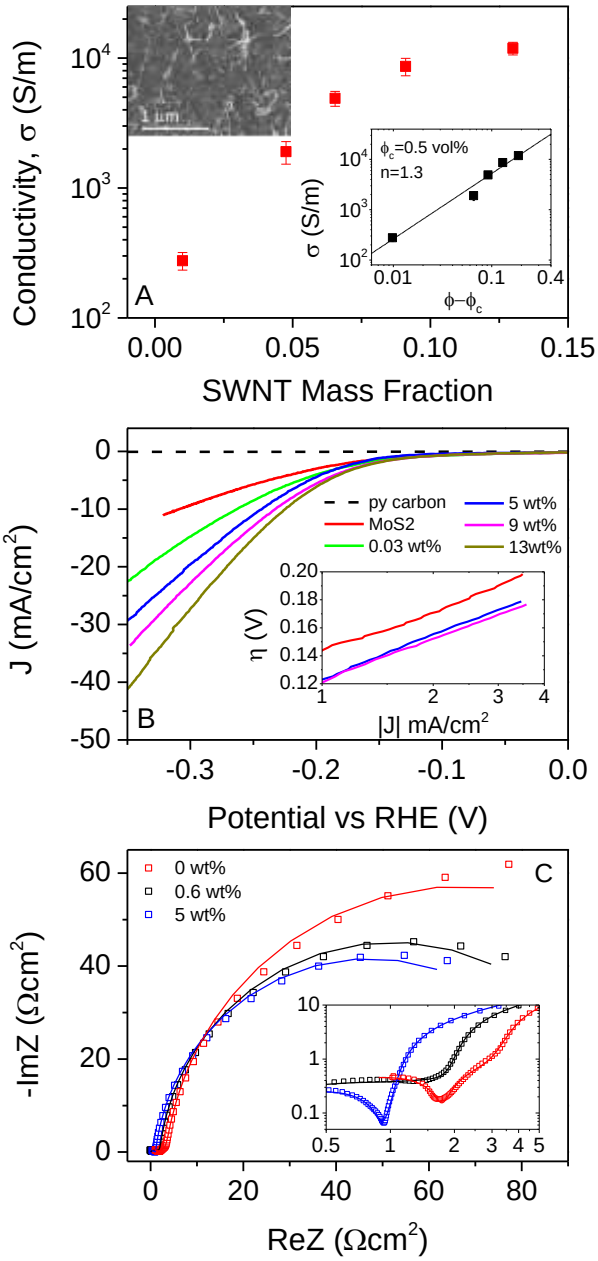

Figure 4: (A) In-plane electrical conductivity, σ, of composite films (MoS_2/SWNTs) plotted *versus* SWNT mass fraction. Inset bottom right: percolation analysis of composite films, σ plotted *versus* SWNT volume fraction, ϕ minus the percolation threshold, $\phi_{c,e}$. The volume fraction was estimated used a mean film density of 2660 kg/m^3. The line is fit to percolation theory equation 11. Inset top left: SEM image of MoS_2/SWNT composite film with 13 wt% loading of SWNTs. The images of the composite films suggest effective mixing of the two components. (B) Polarization curves of MoS_2/SWNT composites (~1.45 mg/cm^2 MoS_2) with SWNT weight percent ranging from 0 wt% to 13 wt%. Higher current densities are obtained with the addition of a few wt% SWNT. Inset: corresponding Tafel plots. In all cases the mass per area of MoS_2 was kept constant at 1.45 mg/cm^2. (C) Impedance spectroscopy data plotted

as Nyquist plots for an MoS_2-only electrode and two composite electrodes. The lines are fits to the model described in the SI. All impedance spectra were collected at an overpotential of 150 mV. The inset shows the high frequency regime plotted on a log-log scale.

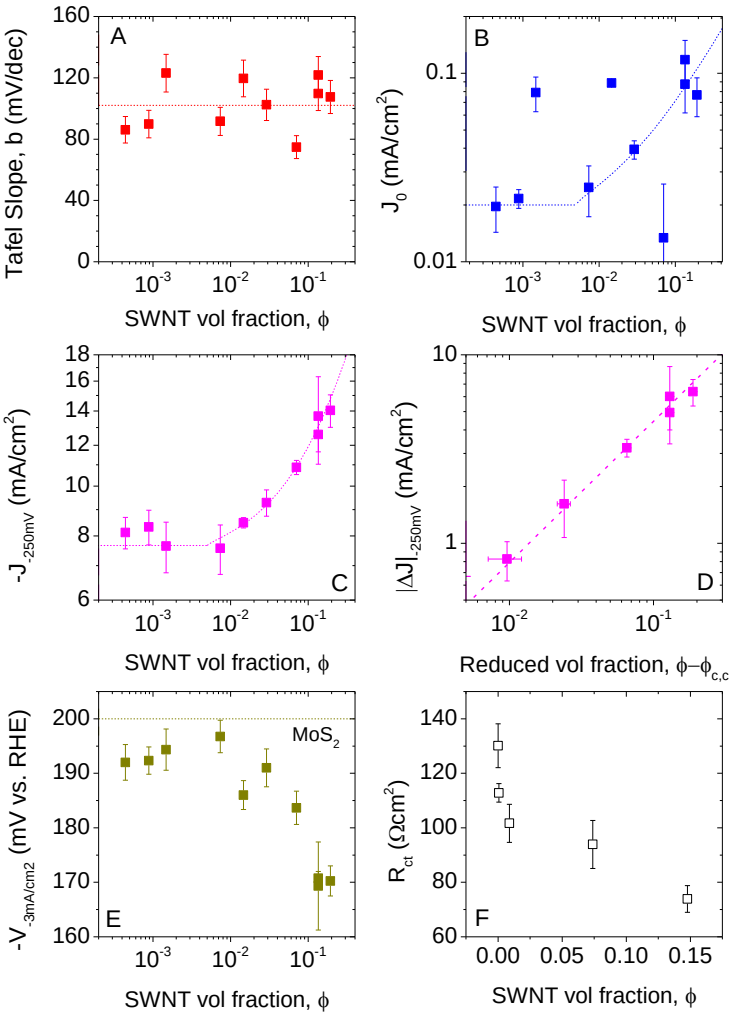

Figure 5: Relationship between electrocatalytic performance and SWNT volume fraction, ϕ, of MoS_2/SWNT composite films with 1.45 mg/cm^2 of MoS_2 (t~5 μm). (A) Tafel slope *versus* ϕ. There is no significant change in Tafel slope with increasing ϕ, with average slope of b~102±17 mV/dec. (B) Exchange current density *versus* SWNT volume fraction ϕ. (C) Current density measured at a potential of -250 mV vs RHE plotted *versus* SWNT volume fraction ϕ. (D) Percolation plot of $|\Delta J|_{-250mV} = -(J_{-250mV} - J^{MoS2}_{-250mV})$ *versus* ϕ-$\phi_{c,c}$, with $\phi_{c,c}$=0.5 vol% and J^{MoS2}_{-250mV} =-7.7 mA/cm^2. (E) Potential required to achieve a current density of -3 mA/cm^2 plotted

versus SWNT volume fraction, ϕ. (F) Charge transfer resistance, as measured by impedance, plotted *versus* SWNT volume fraction, ϕ.

References

1. Zhang, Q.; Uchaker, E.; Candelaria, S. L.; Cao, G., Nanomaterials for Energy Conversion and Storage. *Chem. Soc. Rev.* **2013,** 42, 3127-3171.
2. Gong, M.; Zhou, W.; Tsai, M. C.; Zhou, J.; Guan, M.; Lin, M. C.; Zhang, B.; Hu, Y.; Wang, D. Y.; Yang, J., *et al.*, Nanoscale Nickel Oxide/Nickel Heterostructures for Active Hydrogen Evolution Electrocatalysis. *Nat Commun* **2014,** 5, 4695.
3. Voiry, D.; Yamaguchi, H.; Li, J. W.; Silva, R.; Alves, D. C. B.; Fujita, T.; Chen, M. W.; Asefa, T.; Shenoy, V. B.; Eda, G., *et al.*, Enhanced Catalytic Activity in Strained Chemically Exfoliated WS_2 Nanosheets for Hydrogen Evolution. *Nat. Mater.* **2013,** 12, 850-855.
4. Winther-Jensen, B.; Fraser, K.; Ong, C.; Forsyth, M.; MacFarlane, D. R., Conducting Polymer Composite Materials for Hydrogen Generation. *Adv. Mater.* **2010,** 22, 1727-1730.
5. Chhowalla, M.; Shin, H. S.; Eda, G.; Li, L.-J.; Loh, K. P.; Zhang, H., The Chemistry of Two-Dimensional Layered Transition Metal Dichalcogenide Nanosheets. *Nature Chem.* **2013,** 5, 263-275.
6. Wang, Q. H.; Kalantar-Zadeh, K.; Kis, A.; Coleman, J. N.; Strano, M. S., Electronics and Optoelectronics of Two-Dimensional Transition Metal Dichalcogenides. *Nat. Nanotechnol.* **2012,** 7, 699-712.
7. Liu, J.; Liu, X. W., Two-Dimensional Nanoarchitectures for Lithium Storage. *Adv Mater* **2012,** 24, 4097-111.
8. Yang, J.; Shin, H. S., Recent Advances in Layered Transition Metal Dichalcogenides for Hydrogen Evolution Reaction. *J. Mater. Chem. A* **2014,** 2, 5979-5985.
9. Higgins, T. M.; McAteer, D.; Coelho, J. C. M.; Sanchez, B. M.; Gholamvand, Z.; Moriarty, G.; McEvoy, N.; Berner, N. C.; Duesberg, G. S.; Nicolosi, V., *et al.*, Effect of Percolation on the Capacitance of Supercapacitor Electrodes Prepared from Composites of Manganese Dioxide Nanoplatelets and Carbon Nanotubes. *ACS Nano* **2014,** 8, 9567-9579.
10. Stephenson, T.; Li, Z.; Olsen, B.; Mitlin, D., Lithium Ion Battery Applications of Molybdenum Disulfide (MoS_2) Nanocomposites. *Energy Environ. Sci.* **2014,** 7, 209-231.
11. Wu, M.; Wang, Y.; Lin, X.; Yu, N.; Wang, L.; Wang, L.; Hagfeldt, A.; Ma, T., Economical and Effective Sulfide Catalysts for Dye-Sensitized Solar Cells as Counter Electrodes. *Phys. Chem. Chem. Phys.* **2011,** 13, 19298-19301.
12. Kong, D.; Wang, H.; Cha, J. J.; Pasta, M.; Koski, K. J.; Yao, J.; Cui, Y., Synthesis of MoS_2 and $MoSe_2$ Films with Vertically Aligned Layers. *Nano Lett.* **2013,** 13, 1341-7.
13. Wang, H.; Kong, D.; Johanes, P.; Cha, J. J.; Zheng, G.; Yan, K.; Liu, N.; Cui, Y., $MoSe_2$ and WSe_2 Nanofilms with Vertically Aligned Molecular Layers on Curved and Rough Surfaces. *Nano Lett.* **2013,** 13, 3426-33.
14. Merki, D.; Hu, X., Recent Developments of Molybdenum and Tungsten Sulfides as Hydrogen Evolution Catalysts. *Energy Environ. Sci.* **2011,** 4, 3878.
15. Cheng, L.; Huang, W.; Gong, Q.; Liu, C.; Liu, Z.; Li, Y.; Dai, H., Ultrathin WS_2 Nanoflakes as a High-Performance Electrocatalyst for the Hydrogen Evolution Reaction. *Angew. Chem.* **2014,** 126, 7994-7997.
16. Nicolosi, V.; Chhowalla, M.; Kanatzidis, M. G.; Strano, M. S.; Coleman, J. N., Liquid Exfoliation of Layered Materials. *Science* **2013,** 340, 122641.
17. Jaegermann, W.; Tributsch, H., Interfacial Properties of Semiconducting Transition-Metal Chalcogenides. *Prog. Surf. Sci.* **1988,** 29, 1-167.
18. Laursen, A. B.; Kegnæs, S.; Dahl, S.; Chorkendorff, I., Molybdenum Sulfides-Efficient and Viable Materials for Electro - and Photoelectrocatalytic Hydrogen Evolution. *Energy Environ. Sci.* **2012,** 5, 5577.
19. Ge, P. Y.; Scanlon, M. D.; Peljo, P.; Bian, X. J.; Vubrel, H.; O'Neill, A.; Coleman, J. N.; Cantoni, M.; Hu, X. L.; Kontturi, K., *et al.*, Hydrogen Evolution Across Nano-Schottky Junctions at

Carbon Supported MoS_2 Catalysts in Biphasic Liquid Systems. *Chem. Commun.* **2012,** 48, 6484-6486.
20. Voiry, D.; Salehi, M.; Silva, R.; Fujita, T.; Chen, M.; Asefa, T.; Shenoy, V. B.; Eda, G.; Chhowalla, M., Conducting MoS(2) Nanosheets as Catalysts for Hydrogen Evolution Reaction. *Nano Lett.* **2013,** 13, 6222-7.
21. Ji, S.; Yang, Z.; Zhang, C.; Liu, Z.; Tjiu, W. W.; Phang, I. Y.; Zhang, Z.; Pan, J.; Liu, T., Exfoliated MoS_2 Nanosheets as Efficient Catalysts for Electrochemical Hydrogen Evolution. *Electrochim. Acta* **2013,** 109, 269-275.
22. Lukowski, M. A.; Daniel, A. S.; Meng, F.; Forticaux, A.; Li, L.; Jin, S., Enhanced Hydrogen Evolution Catalysis from Chemically Exfoliated Metallic MoS_2 Nanosheets. *J. Am. Chem. Soc.* **2013,** 135, 10274-7.
23. Zhang, K.; Zhao, Y.; Zhang, S.; Yu, H.; Chen, Y.; Gao, P.; Zhu, C., MoS_2 Nanosheet/Mo2C-Embedded N-Doped Carbon Nanotubes: Synthesis and Electrocatalytic Hydrogen Evolution Performance. *J. Mater. Chem. A* **2014,** 2, 18715-18719.
24. Nolan, H.; McEvoy, N.; O'Brien, M.; Berner, N. C.; Yim, C.; Hallam, T.; McDonald, A. R.; Duesberg, G. S., Molybdenum Disulfide/Pyrolytic Carbon Hybrid Electrodes for Scalable Hydrogen Evolution. *Nanoscale* **2014,** 6, 8185-91.
25. Shi, J.; Ma, D.; Han, G.-F.; Zhang, Y.; Ji, Q.; Gao, T.; Sun, J.; Song, X.; Li, C.; Zhang, Y., *et al.*, Controllable Growth and Transfer of Mono layer MoS_2 on Au Foils and Its Potential Application in Hydrogen Evolution Reaction. *ACS Nano* **2014,** 8, 10196-10204.
26. Tsai, C.; Abild-Pedersen, F.; Norskov, J. K., Tuning the MoS_2 Edge-Site Activity for Hydrogen Evolution via Support Interactions. *Nano Lett.* **2014,** 14, 1381-1387.
27. Hinnemann, B.; Moses, P. G.; Bonde, J.; Jorgensen, K. P.; Nielsen, J. H.; Horch, S.; Chorkendorff, I.; Norskov, J. K., Biomimetic Hydrogen Evolution: MoS_2 Nanoparticles as Catalyst for Hydrogen Evolution. *J. Am. Chem. Soc.* **2005,** 127, 5308-9.
28. Jaramillo, T. F.; Jorgensen, K. P.; Bonde, J.; Nielsen, J. H.; Horch, S.; Chorkendorff, I., Identification of Active Edge Sites for Electrochemical H2 Evolution from MoS_2 Nanocatalysts. *Science* **2007,** 317, 100-102.
29. Lassalle-Kaiser, B.; Merki, D.; Vrubel, H.; Gul, S.; Yachandra, V. K.; Hu, X. L.; Yano, J., Evidence from in Situ X-ray Absorption Spectroscopy for the Involvement of Terminal Disulfide in the Reduction of Protons by an Amorphous Molybdenum Sulfide Electrocatalyst. *J. Am. Chem. Soc.* **2015,** 137, 314-321.
30. Coleman, J. N., Liquid-Phase Exfoliation of Nanotubes and Graphene. *Adv. Funct. Mater.* **2009,** 19, 3680-3695.
31. Paton, K. R.; Varrla, E.; Backes, C.; Smith, R. J.; Khan, U.; O'Neill, A.; Boland, C.; Lotya, M.; Istrate, O. M.; King, P., *et al.*, Scalable Production of Large Quantities of Defect-Free Few-Layer Graphene by Shear Exfoliation in Liquids. *Nat. Mater.* **2014,** 13, 624-630.
32. Varrla, E.; Backes, C.; Paton, K. R.; Harvey, A.; Gholamvand, Z.; McCauley, J.; Coleman, J. N., Large-Scale Production of Size-Controlled MoS2Nanosheets by Shear Exfoliation. *Chemistry of Materials* **2015,** 27, 1129-1139.
33. Nguyen, E. P.; Carey, B. J.; Daeneke, T.; Ou, J. Z.; Latham, K.; Zhuiykov, S.; Kalantar-zadeh, K., Investigation of Two-Solvent Grinding-Assisted Liquid Phase Exfoliation of Layered MoS_2. *Chem. Mater.* **2015,** 27, 53-59.
34. Backes, C.; Smith, R. J.; McEvoy, N.; Berner, N. C.; McCloskey, D.; Nerl, H. C.; O'Neill, A.; King, P. J.; Higgins, T.; Hanlon, D., *et al.*, Edge and Confinement Effects Allow in situ Measurement of Size and Thickness of Liquid-Exfoliated Nanosheets. *Nat Commun* **2014,** 5, 4576.
35. Coleman, J. N.; Lotya, M.; O'Neill, A.; Bergin, S. D.; King, P. J.; Khan, U.; Young, K.; Gaucher, A.; De, S.; Smith, R. J., *et al.*, Two-Dimensional Nanosheets Produced by Liquid Exfoliation of Layered Materials. *Science* **2011,** 331, 568-571.
36. Harvey, A.; Backes, C.; Gholamvand, Z.; Hanlon, D.; McAteer, D.; Nerl, H. C.; McGuire, E.; Seral-Ascaso, A.; Ramasse, Q. M.; McEvoy, N., *et al.*, Preparation of Gallium Sulfide Nanosheets by Liquid Exfoliation and Their Application As Hydrogen Evolution Catalysts. *Chem. Mater.* **2015,** 27, 3483-3493.
37. Zhao, X.; Zhu, H.; Yang, X., Amorphous Carbon Supported MoS(2) Nanosheets as Effective Catalysts for Electrocatalytic Hydrogen Evolution. *Nanoscale* **2014,** 6, 10680-5.

38. Zhang, N.; Gan, S.; Wu, T.; Ma, W.; Han, D.; Niu, L., Growth Control of MoS_2 Nanosheets on Carbon Cloth for Maximum Active Edges Exposed: An Excellent Hydrogen Evolution 3D Cathode. *ACS Appl. Mater. Interfaces* **2015,** 7, 12193-202.
39. Yu, H.; Yu, X.; Chen, Y.; Zhang, S.; Gao, P.; Li, C., A Strategy to Synergistically Increase the Number of Active Edge Sites and the Conductivity of MoS_2 Nanosheets for Hydrogen Evolution. *Nanoscale* **2015,** 7, 8731-8.
40. Li, Y.; Wang, H.; Xie, L.; Liang, Y.; Hong, G.; Dai, H., MoS_2 Nanoparticles Grown on Graphene: an Advanced Catalyst for the Hydrogen Evolution Reaction. *J. Am. Chem. Soc.* **2011,** 133, 7296-9.
41. Xie, J.; Zhang, J.; Li, S.; Grote, F.; Zhang, X.; Zhang, H.; Wang, R.; Lei, Y.; Pan, B.; Xie, Y., Controllable Disorder Engineering in Oxygen-Incorporated MoS_2 Ultrathin Nanosheets for Efficient Hydrogen Evolution. *J. Am. Chem. Soc.* **2013,** 135, 17881-8.
42. Wang, T.; Gao, D.; Zhuo, J.; Zhu, Z.; Papakonstantinou, P.; Li, Y.; Li, M., Size-Dependent Enhancement of Electrocatalytic Oxygen-Reduction and Hydrogen-Evolution Performance of MoS_2 Particles. *Chem.--Eur. J.* **2013,** 19, 11939-48.
43. Wang, H.; Lu, Z.; Xu, S.; Kong, D.; Cha, J. J.; Zheng, G.; Hsu, P. C.; Yan, K.; Bradshaw, D.; Prinz, F. B., *et al.*, Electrochemical Tuning of Vertically Aligned MoS_2 Nanofilms and its Application in Improving Hydrogen Evolution Reaction. *Proc. Natl. Acad. Sci. U. S. A.* **2013,** 110, 19701-6.
44. Chung, D. Y.; Park, S. K.; Chung, Y. H.; Yu, S. H.; Lim, D. H.; Jung, N.; Ham, H. C.; Park, H. Y.; Piao, Y.; Yoo, S. J., *et al.*, Edge-Exposed MoS_2 Nano-Assembled Structures as Efficient Electrocatalysts for Hydrogen Evolution Reaction. *Nanoscale* **2014,** 6, 2131-6.
45. Benson, J.; Li, M.; Wang, S.; Wang, P.; Papakonstantinou, P., Electrocatalytic Hydrogen Evolution Reaction on Edges of a Few Layer Molybdenum Disulfide Nanodots. *ACS Appl. Mater. Interfaces* **2015,** 7, 14113-22.
46. Xie, J.; Zhang, H.; Li, S.; Wang, R.; Sun, X.; Zhou, M.; Zhou, J.; Lou, X. W.; Xie, Y., Defect-Rich MoS_2 Ultrathin Nanosheets with Additional Active Edge Sites for Enhanced Electrocatalytic Hydrogen Evolution. *Adv Mater* **2013,** 25, 5807-13.
47. Merki, D.; Fierro, S.; Vrubel, H.; Hu, X., Amorphous Molybdenum Sulfide Films as Catalysts for Electrochemical Hydrogen Production in Water. *Chem. Sci.* **2011,** 2, 1262-1267.
48. Vrubel, H.; Merki, D.; Hu, X., Hydrogen Evolution Catalyzed by MoS_3 and MoS_2 Particles. *Energy Environ. Sci.* **2012,** 5, 6136.
49. Chen, T.-Y.; Chang, Y.-H.; Hsu, C.-L.; Wei, K.-H.; Chiang, C.-Y.; Li, L.-J., Comparative Study on MoS_2 and WS_2 for Electrocatalytic Water Splitting. *Int. J. Hydrogen Energy* **2013,** 38, 12302-12309.
50. Xia, X.; Zheng, Z.; Zhang, Y.; Zhao, X.; Wang, C., Synthesis of MoS_2-Carbon Composites with Different Morphologies and their Application in Hydrogen Evolution Reaction. *Int. J. Hydrogen Energy* **2014,** 39, 9638-9650.
51. Laursen, A. B.; Vesborg, P. C.; Chorkendorff, I., A High-Porosity Carbon Molybdenum Sulphide Composite with Enhanced Electrochemical Hydrogen Evolution and Stability. *Chem Commun (Camb)* **2013,** 49, 4965-7.
52. Yang, L.; Hong, H.; Fu, Q.; Huang, Y. F.; Zhang, J. Y.; Cui, X. D.; Fan, Z. Y.; Liu, K. H.; Xiang, B., Single-Crystal Atomic-Layered Molybdenum Disulfide Nanobelts with High Surface Activity. *ACS Nano* **2015,** 9, 6478-6483.
53. Zhang, L. M.; Liu, K. H.; Wong, A. B.; Kim, J.; Hong, X. P.; Liu, C.; Cao, T.; Louie, S. G.; Wang, F.; Yang, P. D., Three-Dimensional Spirals of Atomic Layered MoS_2. *Nano Lett.* **2014,** 14, 6418-6423.
54. Kibsgaard, J.; Chen, Z.; Reinecke, B. N.; Jaramillo, T. F., Engineering the surface structure of MoS_2 to preferentially expose active edge sites for electrocatalysis. *Nat. Mater.* **2012,** 11, 963-9.
55. Chang, Y. H.; Lin, C. T.; Chen, T. Y.; Hsu, C. L.; Lee, Y. H.; Zhang, W.; Wei, K. H.; Li, L. J., Highly Efficient Electrocatalytic Hydrogen Production by MoS(x) Grown on Graphene-Protected 3D Ni Foams. *Adv Mater* **2013,** 25, 756-60.
56. Wang, H. T.; Lu, Z. Y.; Kong, D. S.; Sun, J.; Hymel, T. M.; Cui, Y., Electrochemical Tuning of MoS_2 Nanoparticles on Three-Dimensional Substrate for Efficient Hydrogen Evolution. *ACS Nano* **2014,** 8, 4940-4947.

57. Zhang, K.; Zhao, Y.; Zhang, S.; Yu, H.; Chen, Y.; Gao, P.; Zhu, C., MoS2nanosheet/Mo2C-embedded N-doped carbon nanotubes: synthesis and electrocatalytic hydrogen evolution performance. *J. Mater. Chem. A* **2014,** 2, 18715-18719.
58. Bonde, J.; Moses, P. G.; Jaramillo, T. F.; Norskov, J. K.; Chorkendorff, I., Hydrogen Evolution on Nano-Particulate Transition Metal Sulfides. *Faraday Discuss.* **2008,** 140, 219-231.
59. Cunningham, G.; Khan, U.; Backes, C.; Hanlon, D.; McCloskey, D.; Donegan, J. F.; Coleman, J. N., Photoconductivity of Solution-Processed MoS_2 films *J. Mater. Chem. C* **2013,** 1, 6899-6904.
60. Zhu, H.; Lyu, F. L.; Du, M. L.; Zhang, M.; Wane, Q. F.; Yao, J. M.; Guo, B. C., Design of Two-Dimensional, Ultrathin MoS_2 Nanoplates Fabricated Within One-Dimensional Carbon Nanofibers With Thermosensitive Morphology: High-Performance Electrocatalysts for the Hydrogen Evolution Reaction. *ACS Appl. Mater. Interfaces* **2014,** 6, 22126-22137.
61. Liao, L.; Zhu, J.; Bian, X.; Zhu, L.; Scanlon, M. D.; Girault, H. H.; Liu, B., MoS2Formed on Mesoporous Graphene as a Highly Active Catalyst for Hydrogen Evolution. *Advanced Functional Materials* **2013,** 23, 5326-5333.
62. Li, F.; Zhang, L.; Li, J.; Lin, X.; Li, X.; Fang, Y.; Huang, J.; Li, W.; Tian, M.; Jin, J., *et al.*, Synthesis of Cu–MoS_2/rGO Hybrid as Non-Noble Metal Electrocatalysts for the Hydrogen Evolution Reaction. *J. Power Sources* **2015,** 292, 15-22.
63. Youn, D. H.; Han, S.; Kim, J. Y.; Kim, J. Y.; Park, H.; Choi, S. H.; Lee, J. S., Highly Active and Stable Hydrogen Evolution Electrocatalysts Based on Molybdenum Compounds on Carbon Nanotube-Graphene Hybrid Support. *ACS Nano* **2014,** 8, 5164-5173.
64. Dai, X.; Du, K.; Li, Z.; Sun, H.; Yang, Y.; Zhang, W.; Zhang, X., Enhanced Hydrogen Evolution Reaction on Few–Layer MoS_2 Nanosheets–Coated Functionalized Carbon Nanotubes. *Int. J. Hydrogen Energy* **2015,** 40, 8877-8888.
65. Yan, Y.; Ge, X.; Liu, Z.; Wang, J. Y.; Lee, J. M.; Wang, X., Facile Synthesis of Low Crystalline MoS_2 Nanosheet-Coated CNTs for Enhanced Hydrogen Evolution Reaction. *Nanoscale* **2013,** 5, 7768-71.
66. Li, D. J.; Maiti, U. N.; Lim, J.; Choi, D. S.; Lee, W. J.; Oh, Y.; Lee, G. Y.; Kim, S. O., Molybdenum Sulfide/N-Doped CNT Forest Hybrid Catalysts for High-Performance Hydrogen Evolution Reaction. *Nano Lett.* **2014,** 14, 1228-1233.
67. Kim, J.; Byun, S.; Smith, A. J.; Yu, J.; Huang, J., Enhanced Electrocatalytic Properties of Transition-Metal Dichalcogenides Sheets by Spontaneous Gold Nanoparticle Decoration. *The Journal of Physical Chemistry Letters* **2013,** 4, 1227-1232.
68. Cunningham, G.; Lotya, M.; McEvoy, N.; Duesberg, G. S.; van der Schoot, P.; Coleman, J. N., Percolation Scaling in Composites of Exfoliated MoS_2 Filled with Nanotubes and Graphene. *Nanoscale* **2012,** 4, 6260-6264.
69. Khan, U.; O'Connor, I.; Gun'ko, Y. K.; Coleman, J. N., The Preparation of Hybrid Films of Carbon Nanotubes and Nano-Graphite/Graphene with Excellent Mechanical and Electrical Properties. *Carbon* **2010,** 48, 2825-2830.
70. Khan, U.; O'Neill, A.; Lotya, M.; De, S.; Coleman, J. N., High-Concentration Solvent Exfoliation of Graphene. *Small* **2010,** 6, 864-871.
71. Conway, B. E.; Tilak, B. V., Interfacial Processes Involving Electrocatalytic Evolution and Oxidation of H_2, and the Role of Chemisorbed H. *Electrochim. Acta* **2002,** 47, 3571-3594.
72. Tributsch, H.; Bennett, J. C., Electrochemistry and Photochemistry of MoS_2 Layer Crystals .1. *J. Electroanal. Chem.* **1977,** 81, 97-111.
73. Yu, Y.; Huang, S. Y.; Li, Y.; Steinmann, S. N.; Yang, W.; Cao, L., Layer-Dependent Electrocatalysis of MoS_2 for Hydrogen Evolution. *Nano Lett.* **2014,** 14, 553-8.
74. Wang, D.; Wang, Z.; Wang, C.; Zhou, P.; Wu, Z.; Liu, Z., Distorted MoS_2 Nanostructures: An Efficient Catalyst for the Electrochemical Hydrogen Evolution Reaction. *Electrochem. Commun.* **2013,** 34, 219-222.
75. Wu, Z.; Fang, B.; Wang, Z.; Wang, C.; Liu, Z.; Liu, F.; Wang, W.; Alfantazi, A.; Wang, D.; Wilkinson, D. P., MoS2Nanosheets: A Designed Structure with High Active Site Density for the Hydrogen Evolution Reaction. *ACS Catalysis* **2013,** 3, 2101-2107.

76. Chang, Y. H.; Wu, F. Y.; Chen, T. Y.; Hsu, C. L.; Chen, C. H.; Wiryo, F.; Wei, K. H.; Chiang, C. Y.; Li, L. J., Three- Dimensional Molybdenum Sulfi de Sponges for Electrocatalytic Water Splitting. *Small* **2014,** 10, 895-900.
77. Zeng, K.; Zhang, D. K., Recent Progress in Alkaline Water Electrolysis for Hydrogen Production and Applications. *Progr. Energy Combust. Sci.* **2010,** 36, 307-326.
78. Fan, X.-L.; Yang, Y.; Xiao, P.; Lau, W.-M., Site-Specific Catalytic Activity in Exfoliated MoS_2 Single-Layer Polytypes for Hydrogen Evolution: Basal Plane and Edges. *J. Mater. Chem. C.* **2014,** 2, 20545-20551.
79. Chen, Z. B.; Cummins, D.; Reinecke, B. N.; Clark, E.; Sunkara, M. K.; Jaramillo, T. F., Core-shell MoO_3-MoS_2 Nanowires for Hydrogen Evolution: A Functional Design for Electrocatalytic Materials. *Nano Lett.* **2011,** 11, 4168-4175.
80. Benson, J.; Li, M.; Wang, S.; Wang, P.; Papakonstantinou, P., Electrocatalytic Hydrogen Evolution Reaction on Edges of a Few Layer Molybdenum Disulfide Nanodots. *ACS Applied Materials & Interfaces* **2015,** 7, 14113-14122.
81. Cunningham, G.; Hanlon, D.; McEvoy, N.; Duesberg, G. S.; Coleman, J. N., Large Variations in Both Dark- and Photoconductivity in Nanosheet Networks as Nanomaterial is Varied from MoS_2 to WTe_2. *Nanoscale* **2015,** 7, 198-208.
82. Bauhofer, W.; Kovacs, J. Z., A Review and Analysis of Electrical Percolation in Carbon Nanotube Polymer Composites. *Compos. Sci. Technol.* **2009,** 69, 1486-1498.
83. Stauffer, D.; Aharony, A., *Introduction to Percolation Theory*. 2nd ed.; Taylor & Francis: London, 1985.
84. Doherty, E. M.; De, S.; Lyons, P. E.; Shmeliov, A.; Nirmalraj, P. N.; Scardaci, V.; Joimel, J.; Blau, W. J.; Boland, J. J.; Coleman, J. N., The spatial uniformity and electromechanical stability of transparent, conductive films of single walled nanotubes. *Carbon* **2009,** 47, 2466-2473.
85. Doyle, R. L.; Lyons, M. E. G., The Oxygen Evolution Reaction at Hydrous Iron Oxide Films in Base: Kinetics and Mechanism. *Physical and Analytical Electrochemistry (General) - 221st Ecs Meeting* **2013,** 45, 3-19.
86. Wang, J. Z.; Lu, L.; Lotya, M.; Coleman, J. N.; Chou, S. L.; Liu, H. K.; Minett, A. I.; Chen, J., Development of MoS_2-CNT Composite Thin Film from Layered MoS_2 for Lithium Batteries. *Advanced Energy Materials* **2013,** 3, 798-805.
87. Liu, Y.; Hanlon, D.; Harvey, A.; He, L.; Li, Y.; Coleman, J. N., Percolation Scaling of Capacity in High Performance MoS_2/SWNT Composite Lithium Ion Battery Electrodes. **in preparation**.
88. Sykes, M. F.; Glen, M.; Gaunt, D. S., Percolation Probability for Site Problem on Triangular Lattice. *Journal of Physics a-Mathematical and General* **1974,** 7, L105-L108.
89. McEvoy, N.; Peltekis, N.; Kumar, S.; Rezvani, E.; Nolan, H.; Keeley, G. P.; Blau, W. J.; Duesberg, G. S., Synthesis and Analysis of Thin Conducting Pyrolytic Carbon Films. *Carbon* **2012,** 50, 1216-1226.